Article

Cell Reports

MCUR1 Is a Scaffold Factor for the MCU Complex Function and Promotes Mitochondrial Bioenergetics

Graphical Abstract

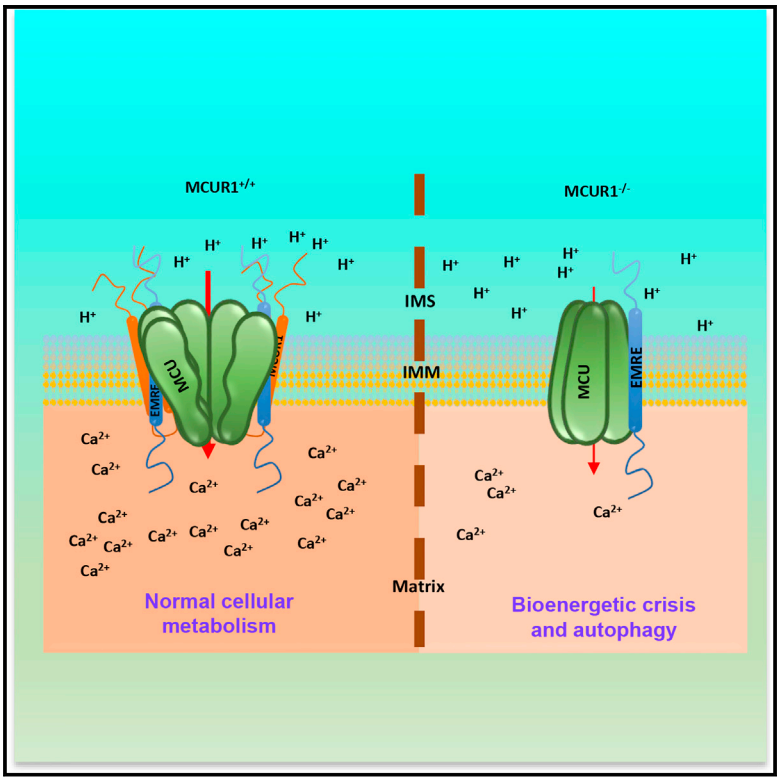

Authors

Dhanendra Tomar, Zhiwei Dong, Santhanam Shanmughapriya, ..., John W. Elrod, Sudarsan Rajan, Muniswamy Madesh

Correspondence

madeshm@temple.edu

In Brief

Tomar et al. show that genetic ablation of the MCU complex component MCUR1 perturbs MCU heterooligomeric complex and impairs mitochondrial Ca^{2+} uptake. MCUR1 binds to MCU and EMRE and functions as a scaffold factor that is necessary for proper Ca^{2+}-dependent mitochondrial bioenergetics.

Highlights

- MCUR1 binds to MCU and EMRE and functions as a scaffold factor
- The coiled-coil domains of both MCU and MCUR1 are essential for MCU complex assembly
- Genetic deletion of MCUR1 severely impairs $[Ca^{2+}]_m$ uptake and I_{MCU} current
- MCUR1 deletion impairs bioenergetics and cell migration and elicits autophagy

Tomar et al., 2016, Cell Reports *15*, 1673–1685
May 24, 2016
http://dx.doi.org/10.1016/j.celrep.2016.04.050

Cell Reports
Article

MCUR1 Is a Scaffold Factor for the MCU Complex Function and Promotes Mitochondrial Bioenergetics

Dhanendra Tomar,[1,2,11] Zhiwei Dong,[1,2,10,11] Santhanam Shanmughapriya,[1,2,11] Diana A. Koch,[2,3,11] Toby Thomas,[1,2] Nicholas E. Hoffman,[1,2] Shrishiv A. Timbalia,[4] Samuel J. Goldman,[1,2] Sarah L. Breves,[1,2] Daniel P. Corbally,[1,2] Neeharika Nemani,[1,2] Joseph P. Fairweather,[1,2] Allison R. Cutri,[1,2] Xueqian Zhang,[2] Jianliang Song,[2] Fabián Jaña,[1,2] Jianhe Huang,[5] Carlos Barrero,[6] Joseph E. Rabinowitz,[2] Timothy S. Luongo,[2] Sarah M. Schumacher,[2] Michael E. Rockman,[1,2] Alexander Dietrich,[3] Salim Merali,[6] Jeffrey Caplan,[7] Peter Stathopulos,[8] Rexford S. Ahima,[9] Joseph Y. Cheung,[2] Steven R. Houser,[5] Walter J. Koch,[2] Vickas Patel,[5] Vishal M. Gohil,[4] John W. Elrod,[2] Sudarsan Rajan,[1,2] and Muniswamy Madesh[1,2,*]

[1]Department of Medical Genetics and Molecular Biochemistry, Lewis Katz School of Medicine at Temple University, Philadelphia, PA 19140, USA
[2]Center for Translational Medicine, Lewis Katz School of Medicine at Temple University, Philadelphia, PA 19140, USA
[3]Walther Straub Institute for Pharmacology and Toxicology, Member of the German Center for Lung Research (DZL), School of Medicine, LM University of Munich, Nussbaumstrasse 26, 80336 Munich, Germany
[4]Department of Biochemistry and Biophysics, Texas A&M University, College Station, TX 77843, USA
[5]Cardiovascular Research Center and Departments of Medicine and Physiology, Temple University, Philadelphia, PA 19140, USA
[6]Department of Pharmaceutical Sciences, Temple University, Philadelphia, PA 19140, USA
[7]Department of Biological Sciences, Delaware Biotechnology Institute, University of Delaware, Newark, DE 19711, USA
[8]Department of Physiology and Pharmacology, Western University, London, ON N6A 5C1, Canada
[9]Department of Medicine, Division of Endocrinology, Diabetes and Metabolism, Perelman School of Medicine, University of Pennsylvania, Philadelphia, PA 19104, USA
[10]Institute of Burn Research, Southwest Hospital, State Key Laboratory of Trauma, Burns and Combined Injury, Third Military Medical University, Chongqing 400038, People's Republic of China
[11]Co-first author
*Correspondence: madeshm@temple.edu
http://dx.doi.org/10.1016/j.celrep.2016.04.050

SUMMARY

Mitochondrial Ca^{2+} Uniporter (MCU)-dependent mitochondrial Ca^{2+} uptake is the primary mechanism for increasing matrix Ca^{2+} in most cell types. However, a limited understanding of the MCU complex assembly impedes the comprehension of the precise mechanisms underlying MCU activity. Here, we report that mouse cardiomyocytes and endothelial cells lacking MCU regulator 1 (MCUR1) have severely impaired $[Ca^{2+}]_m$ uptake and I_{MCU} current. MCUR1 binds to MCU and EMRE and function as a scaffold factor. Our protein binding analyses identified the minimal, highly conserved regions of coiled-coil domain of both MCU and MCUR1 that are necessary for heterooligomeric complex formation. Loss of MCUR1 perturbed MCU heterooligomeric complex and functions as a scaffold factor for the assembly of MCU complex. Vascular endothelial deletion of MCU and MCUR1 impaired mitochondrial bioenergetics, cell proliferation, and migration but elicited autophagy. These studies establish the existence of a MCU complex that assembles at the mitochondrial integral membrane and regulates Ca^{2+}-dependent mitochondrial metabolism.

INTRODUCTION

The mitochondrial Ca^{2+} uniporter (MCU) is a multimeric complex that mediates the rapid uptake of cytosolic Ca^{2+} from intracellular store release. Rapid mitochondrial Ca^{2+} ($[Ca^{2+}]_m$) uptake is essential for mitochondrial functions, including ATP production and various cellular signaling processes (Babcock et al., 1997; Drago et al., 2011; Duchen, 2000; Glancy and Balaban, 2012; Hajnóczky et al., 1995; O'Rourke, 2007; Rizzuto et al., 2012). Although MCU is a highly selective Ca^{2+} channel, the precise physiological role and the molecular structure of the mitochondrial Ca^{2+} uniporter complex still has to be determined (Kamer and Mootha, 2015; Kirichok et al., 2004). The defining feature of MCU as a channel is that it is activated by finite cytosolic Ca^{2+} ($[Ca^{2+}]_c$) and driven by mitochondrial membrane potential ($\Delta\Psi_m$) and pH (Csordás et al., 2013; Gunter and Pfeiffer, 1990; Mallilankaraman et al., 2012b; Nicholls, 2005; Santo-Domingo and Demaurex, 2012). The original biophysical study revealed that MCU-mediated Ca^{2+} uptake is dependent upon the $\Delta\Psi_m$ (approximately −160 mV) and that mitochondrial Ca^{2+} uniporter current (I_{MCU}) is inwardly rectifying, with a high half-saturation of ~20 mM $[Ca^{2+}]_c$ (Kirichok et al., 2004). Given that the discovery of MCU and its regulators MICU1, MICU2

(mitochondrial Ca^{2+} uptake), MCUR1 (MCU regulator 1), MCUb, and EMRE (essential MCU regulator), there has been considerable interest and uncertainty about how these components constitute and determine MCU activity (Baughman et al., 2011; De Stefani et al., 2011; Mallilankaraman et al., 2012a; Perocchi et al., 2010; Plovanich et al., 2013; Raffaello et al., 2013; Sancak et al., 2013). The active-state transport of Ca^{2+} into the mitochondria is facilitated by MCU and is enhanced by MCUR1 (Mallilankaraman et al., 2012a; Vais et al., 2015). Interestingly, even though excitable and nonexcitable cells express mitochondrial Ca^{2+} uniporter complex components ubiquitously, I_{MCU} activity is differentially controlled (Carafoli and Lehninger, 1971; Fieni et al., 2012; Kwong et al., 2015; Luongo et al., 2015; Pan et al., 2013; Rasmussen et al., 2015; Williams et al., 2013). MCU regulators play a key role in the regulation of tissue-specific mitochondrial Ca^{2+} uptake. However, until now, only the MICU1-MICU2-mediated molecular mechanism of MCU regulation has been deciphered (Csordás et al., 2013; Hoffman et al., 2013; Kamer and Mootha, 2014; Mallilankaraman et al., 2012b; Petrungaro et al., 2015). The question still remains regarding how other regulators of MCU control MCU activity. MCUR1 is originally identified as regulator of MCU in the screening of 45 integral mitochondrial proteins. Recent work on MCUR1 was proposed as a cytochrome c oxidase (COX) assembly factor (Paupe et al., 2015). Here, we show that tissue-specific deletion of MCUR1 in mice resulted in decreased MCU-mediated $[Ca^{2+}]_m$ uptake. We have used various biochemical tools to decipher the mechanism of MCUR1-mediated regulation of MCU activity and mitochondrial bioenergetics.

RESULTS

Deletion of MCUR1 in the Heart and Vasculature Regulates MCU-Dependent $[Ca^{2+}]_m$ Uptake

To investigate the regulatory role of MCUR1 in MCU-mediated $[Ca^{2+}]_m$ uptake in vivo, we generated tissue-specific MCUR1 null mice. Additionally, we investigated MCU- and MCUR1-interacting domains that are required for MCU complex assembly.

To study the function of MCU complex component MCUR1 in highly oxidative phosphorylation (OXPHOS) and moderate OXPHOS-dependent cell types, we generated cardiac- and endothelial-specific knockout (KO) mice models (Figures S1A–S1F). Although cardiac and endothelial MCUR1-deficient mice in the C57BL/6 background were viable, and the expected Mendelian ratios postnatally were similar, we observed fewer cardiac MCUR1-deficient ($MCUR1^{fl/fl}$α-MHCCre; cMCUR1 KO) mice—but not endothelial MCUR1-deficient ($MCUR1^{fl/fl}$VE-Cad-Cre; $MCUR1^{\Delta EC}$) mice—that were also smaller and died 3 weeks after birth. For mechanistic and functional studies, viable cMCUR1 KO mice were used. Similar to $MCUR1^{\Delta EC}$, germline deletion of MCU in endothelial cells did not result in any discernable phenotype (Figures S1A–S1F). Assessment of control, $MCUR1^{\Delta EC}$, and cMCUR1 KO mice showed similar 24-hr metabolic profiles and serum chemistry, although the resting heat production was higher in $MCUR1^{\Delta EC}$ (Figures S1G–S1N). To examine the effect of MCUR1 in MCU-mediated $[Ca^{2+}]_m$ uptake, freshly isolated cardiomyocytes from $MCUR1^{fl/fl}$ (Figures 1A and 1B, black), αMHCCre (Figures 1A and 1B, red), and cMCUR1 KO (Figures 1A and 1B, green) were permeabilized, and $[Ca^{2+}]_m$ uptake was measured. cMCUR1 KO mitochondria showed almost no $[Ca^{2+}]_m$ uptake in response to extramitochondrial Ca^{2+} pulses (Figures 1A and 1B). Similar to cardiomyocytes, endothelial cells or fibroblasts lacking either MCUR1 or MCU resulted in nominal $[Ca^{2+}]_m$ uptake (Figures 1C and 1D and S1O–S1Q). However, mitochondrial membrane potential ($\Delta\Psi_m$) was unchanged in cells lacking both MCU and MCUR1 (Figures S1R–S1T). To determine whether MCUR1 has a role in suppressing I_{MCU} currents, cardiac mitochondria were isolated from $MCUR1^{fl/fl}$, α-MHCCre, and cMCUR1 KO mice, and mitoplasts were subjected to I_{MCU} current recording (Hoffman et al., 2013; Kirichok et al., 2004). cMCUR1 KO mitochondria showed a marked decrease of I_{MCU} current; collectively, these data provide genetic evidence that MCUR1 controls I_{MCU} current and MCU-dependent $[Ca^{2+}]_m$ uptake (Figures 1E and 1F). Importantly, the resting $[Ca^{2+}]_m$ was reduced in endothelial cells lacking MCUR1 and MCU (Figures S1V and S1W) but not in cardiomyocytes lacking MCUR1 (Figure S1U). Because MCU and MCUR1 control $[Ca^{2+}]_m$ uptake, mitochondrial Ca^{2+} handling could impact endothelial proliferation and migration, which are key functions of angiogenesis during wound healing (Davidson and Duchen, 2007). To determine whether proliferation and migration are altered in these mice, primary endothelial cells obtained from $MCUR1^{\Delta EC}$ and $MCU^{\Delta EC}$ were assessed by flow cytometry and scratch assay. Endothelial cell proliferative index and migratory capacity were attenuated in the $MCUR1^{\Delta EC}$ and $MCU^{\Delta EC}$, suggesting perturbation of Ca^{2+} flux between cytosol and mitochondria (Figures 1G and 1H). Given that Ca^{2+} signaling is essential for cell migration, mitochondrial biogenesis, bioenergetics, and dynamics-related component abundance were examined. Loss of MCUR1 had no detectable effect on mitochondrial metabolic protein profiles and OXPHOS complex components (Figures 1I and S1X–S1Z).

MCUR1 Directly Binds MCU and EMRE to Form Active MCU Complex

Because the functional MCU complex and core signaling system are composed of an oligomeric MCU and a family of essential regulators, we tested whether mitochondrial localized MCUR1 modulates MCU activity through a protein-protein interaction. To test this, we conducted immuno-affinity binding followed by quantitative mass spectrometry (MS) analysis. First, HEK293T cells stably expressing MCUR1-FLAG were generated, and cell lysates were immunoprecipitated with FLAG-antibody-conjugated beads. The stringently washed, immunoprecipitated samples were subjected to MS. Three independent pooled samples were able to identify MCUR1 as a component of MCU complex (Figures S2A and S2B; Table S1). To further confirm the endogenous binding partners of MCUR1, we first generated C-terminal V5-tagged MCUR1 and FLAG-tagged MCU, MICU1, CCDC90B, EMRE, and LETM1 plasmid constructs. Individual MCU complex component and LETM1 plasmids were transiently transfected into COS-7 cells, and cell lysates were subjected to immunoprecipitation with V5-antibody. Transfection of COS-7 cells with these tagged proteins showed considerable ectopic protein expression (Figure 2A, top and bottom right). The FLAG-tagged, as well as V5-tagged, individual protein cell lysates were incubated with antibodies specific for V5 to immunoprecipitate the protein complexes. V5-tagged MCUR1 protein was immunoprecipitated, while FLAG-tagged candidate proteins did not

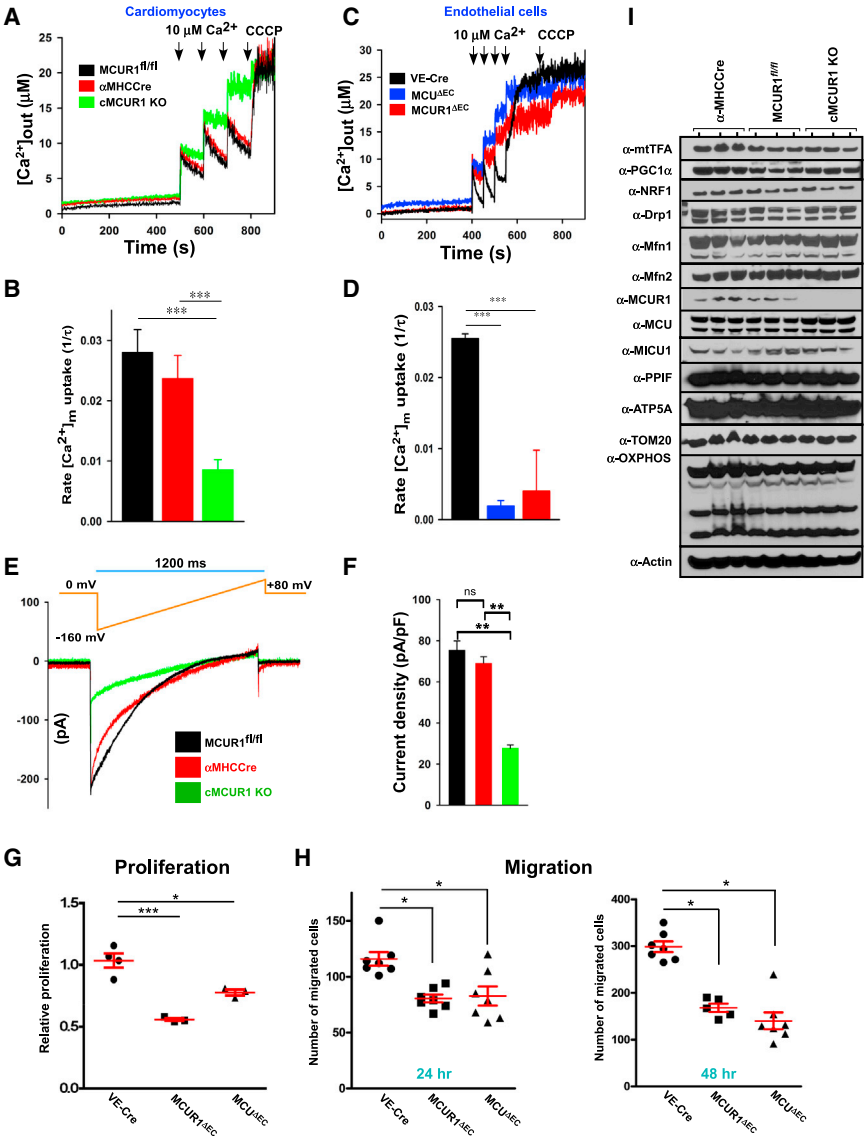

Figure 1. Loss of MCUR1 Impairs MCU-Dependent $[Ca^{2+}]_m$ Uptake and Cell Migration

(A) Cardiomyocytes from mice of the indicated genotypes were isolated and permeabilized with digitonin (80 μg/ml) in intracellular-like media containing thapsigargin (2 μM) and bath $[Ca^{2+}]$ indicator Fura-2FF (1 μM). After reaching steady-state $\Delta\Psi_m$, a series of extramitochondrial Ca^{2+} (10 μM) pulses were added at the indicated time points before adding the mitochondrial uncoupler CCCP (2 μM). Representative traces of extramitochondrial Ca^{2+} ($[Ca^{2+}]_{out}$) clearance by permeabilized cardiomyocytes isolated from $MCUR1^{fl/fl}$ (black), αMHCCre (red), and cMCUR1 KO (green) mice. n = 3.

(B) Mitochondrial Ca^{2+} uptake rate was calculated from traces shown in (A). Data indicate mean ± SEM. ***p < 0.001; n = 3.

(C) Representative traces of $[Ca^{2+}]_{out}$ clearance by permeabilized primary mouse pulmonary vascular endothelial cells (MPVECs) isolated from VE-Cre (black), $MCU^{\Delta EC}$ (blue), and $MCUR1^{\Delta EC}$ (red) mice. 10 μM $[Ca^{2+}]_{out}$ bolus and CCCP (2 μM) were added at the indicated time points. n = 3.

(D) Mitochondrial Ca^{2+} uptake rate was calculated from traces shown in (C). Data indicate mean ± SEM. ***p < 0.001; n = 3.

(E) I_{MCU} current in mitoplasts derived from $MCUR1^{fl/fl}$ (black), αMHCCre (red), and cMCUR1 KO (green) cardiomyocytes. Traces are a representative single recording of I_{MCU}.

(F) I_{MCU} densities (picoamperes per picofarads; pA/pF) in mitoplasts derived from $MCUR1^{fl/fl}$ (black), αMHCCre (red), and cMCUR1 KO (green) cardiomyocytes. Data indicate mean ± SEM. **p < 0.01; ns, not significant; n = 4–7.

(G) Quantification of proliferative index in endothelial cells (ECs) derived from VE-Cre, $MCU^{\Delta EC}$, and $MCUR1^{\Delta EC}$ mice. Data indicate mean ± SEM. *p < 0.05; ***p < 0.001; n = 3–4.

(H) Quantification of gap closure in ECs derived from VE-Cre, $MCU^{\Delta EC}$, and $MCUR1^{\Delta EC}$ mice at 24 and 48 hr. Data indicate mean ± SEM. *p < 0.05; n = 7.

(I) Abundance of indicated mitochondrial proteins in cardiomyocytes derived from αMHCCre, $MCUR1^{fl/fl}$, and cMCUR1 KO mice (n = 3; three mice per group).

pull down, demonstrating antibody specificity (Figure 2A, top and bottom left). Next, we cotransfected MCUR1-V5 with MCU-FLAG, MICU1-FLAG, CCDC90B-FLAG, EMRE-FLAG, and LETM1-FLAG in COS-7 cells. The immunoprecipitation with V5 antibody was able to pull down MCU, CCDC90B, and EMRE-FLAG proteins along with MCUR1 (Figure 2A, top left). Notably, no interaction was seen between MCUR1 and MICU1 or between MCUR1 and LETM1 (Figure 2A, top left). Importantly, MCUR1 binds not only MCU but also EMRE and CCDC90B (Figure 2A). Therefore, we investigated whether CCDC90B also binds with MCU. Similar to the MCUR1 immunoprecipitation protocol, C-terminal hemagglutinin (HA)-tagged CCDC90B was co-transfected with MCU-FLAG, MICU1-FLAG, MCUR1-FLAG, EMRE-FLAG, and LETM1-FLAG in COS-7 cells and investigated their binding by coimmunoprecipitation. Immunoprecipitation of the HA-tagged CCDC90B resulted in strong coimmunoprecipitation of MCU, MCUR1, and EMRE, indicating that both MCUR1 and CCDC90B can interact with MCU components (Figure 2B). We also tested the reciprocal immunoprecipitation using MCU-GFP as bait. C-terminal GFP-tagged MCU was co-transfected with MICU1-FLAG, MCUR1-FLAG, EMRE-FLAG, CCDC90B-FLAG, and LETM1-FLAG in COS-7 cells, and interactions were determined by coimmunoprecipitation. Consistent with MCU as the core component of the MCU complex, MCUR1, EMRE, MICU1, and CCDC90B coimmunoprecipitated with MCU-GFP (Figure 2C). Note that, since MCUR1 undergoes processing, both unprocessed and processed MCUR1 were able to interact with MCU and EMRE. Having observed

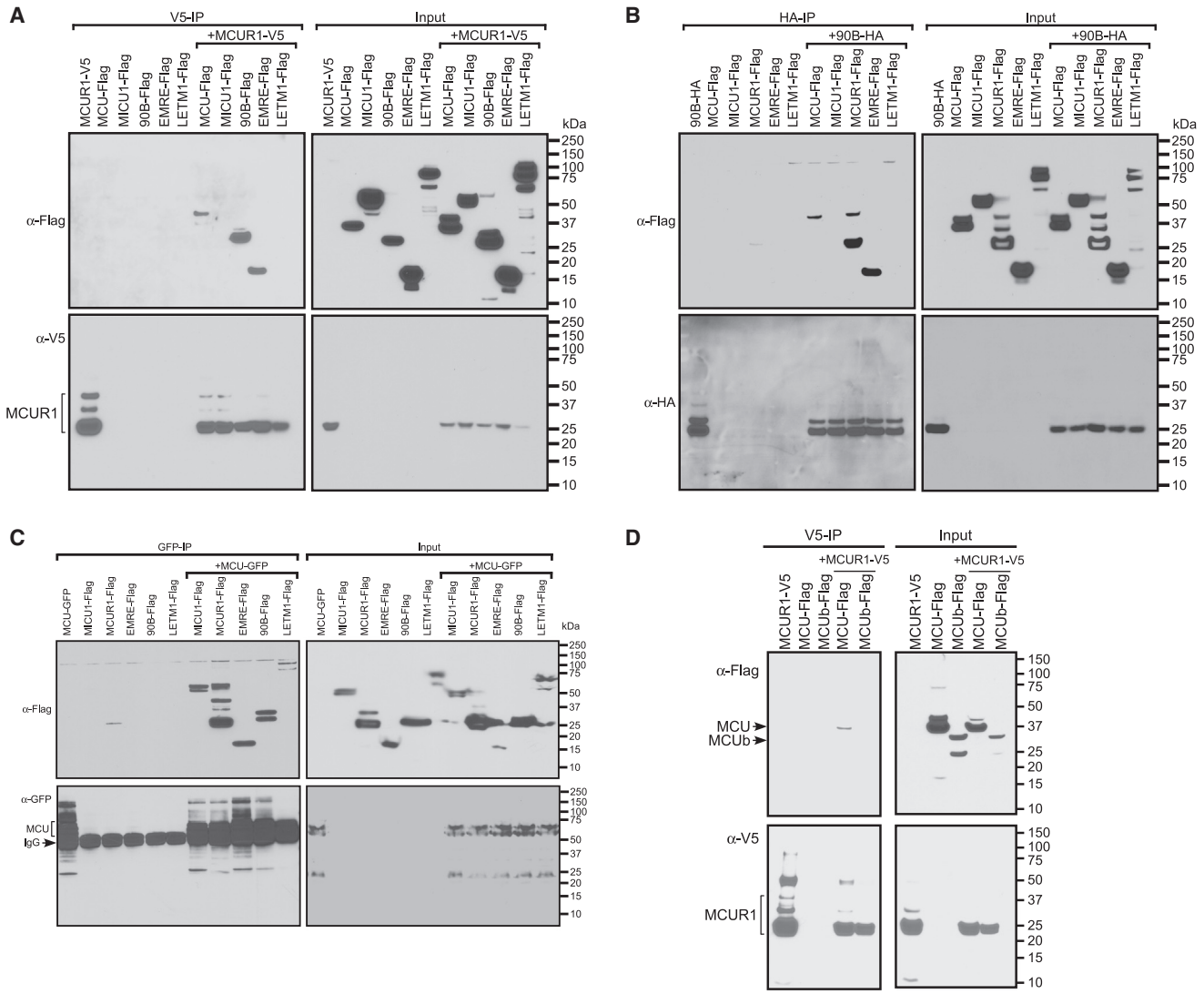

Figure 2. MCUR1 Binds MCU and EMRE

(A) COS-7 cells were transfected with V5-tagged MCUR1 and FLAG-tagged MCU, MICU1, CCDC90B, EMRE, and LETM1 as indicated. Following immunoprecipitation with V5 antibody, total cell lysates and immunoprecipitated materials were subjected to western blot analysis. Cell lysates were probed with anti-FLAG (top right) or anti-V5 (bottom right) antibodies to serve as inputs. Immunoprecipitated samples were probed with anti-FLAG (top left) and anti-V5 (bottom left) antibodies (n = 3).

(B) Western blot analysis of cell lysates (right) or immunoprecipitates (IP; left) from COS-7 cells expressing HA-tagged CCDC90B singly or in combination with FLAG-tagged MCU, MICU1, MCUR1, EMRE, and LETM1 (n = 3).

(C) Western blot analysis of cell lysates (right) or immunoprecipitates (IP; left) from COS-7 cells expressing GFP-tagged MCU and FLAG-tagged MCUR1, MICU1, CCDC90B, EMRE, and LETM1 (n = 3). IgG, immunoglobulin G.

(D) Western blot analysis of cell lysates (right) or immunoprecipitates (IP; left) from COS-7 cells expressing V5-tagged MCUR1 and FLAG-tagged MCU and MCUb (n = 3).

MCUR1 association with LETM1, but not EMRE, by global immunoprecipitation proteomics suggests the endogenous protein abundancy. Our further validation by stringent conventional immunoprecipitation assay revealed MCUR1 to directly bind EMRE, and not LETM1, suggesting an indirect MCUR1-LETM1 interaction. Having observed that CCDC90B binds MCU and MCUR1, we measured the MCU-dependent $[Ca^{2+}]_m$ uptake in CCDC90B knockdown (KD) cells. Silencing of CCDC90B did not alter $[Ca^{2+}]_m$ uptake, suggesting its nominal role in MCU activity (Figures S2C–S2E). As we demonstrated experimentally, the KD of CCDC90B failed to affect the MCU-mediated mitochondrial Ca^{2+} uptake, though it interacts with MCU complex. Additionally, it is important to note that MCU, MICU1, MCUR1, and EMRE are absent in the yeast. However, CCDC90B is present in the yeast and may serve a different function. Furthermore, immunoprecipitation of MCU-GFP was able to pull down MICU1-FLAG, indicating that MCUR1 can bind to MCU and EMRE independent of MICU1. To determine whether MCUR1

binds MCUb, which is a paralogue of MCU, we analyzed the protein-protein interaction of MCUR1 and MCUb by immunoprecipitation. Immunoprecipitation of MCUR1 was able to pull down MCU, but not MCUb, reinforcing that MCUR1 is a specific binding partner of MCU (Figure 2D). Our assessment of MCUb-MCUR1 interactions is based on both immunoprecipitation and MS data, neither of which showed an interaction between these proteins. It is plausible that the stoichiometry of MCU and MCUb may vary in tissues, and future studies are warranted.

Based on these key MCU binding results, we developed an imaging technique, bimolecular fluorescence complementation (BiFC), to visualize and determine MCU complex components on a single-cell basis. BiFC uses a photostable version of two separated yellow fluorescence protein (YFP) fragments (Venus-N155 and Venus-C155) to assess topology-based interactions in live cells. Each fragment on its own is not fluorescent, but upon interaction of the partners, the complex becomes fluorescent (Kodama and Hu, 2010). This technique can also detect recruitment of MCU components to its activation platform making split Venus particularly suitable for real-time imaging, because the association occurs quickly under physiological conditions. To visualize the BiFC protein-protein interaction, live HeLa cells were stained with a $\Delta\Psi_m$ mitochondrial indicator, TMRM. HeLa cells transiently transfected with only one portion of the fluorescent complex, VC155-MCU fragment, remained non-fluorescent (Figures 3A and 3B). MCU-MCU, MCUR1-MCUR1 and MCUR1-EMRE interactions showed fluorescence by complementation due to complex formation and because the split Venus components were on the same side of the inner mitochondrial membrane (IMM). To assess the C-terminal region of EMRE biochemically, C-terminal, FLAG-tagged, EMRE-expressing permeabilized cells were exposed to an outer mitochondrial membrane (OMM) permeabilizing agent, mastoparan, followed by proteinase K (Figure S2F). The BiFC and proteinase K experiments suggest that the MCUR1-EMRE complex formation occurs likely on the intermembrane space side. The MCUR1-MCU, EMRE-MCU, MCUR1-MICU1, and EMRE-MICU1 pairs were unable to reconstitute the fluorescence, because the Venus components were on opposite sides of the IMM (Figures 3A, 3B, and 3F). Similar to the immunoprecipitation protein-protein interaction data, which demonstrated that MICU1 and MCUR1 do not interact, VN155-MCUR1 and VC155-MICU1 failed to display any BiFC fluorescence. Thus, BiFC sequential co-expression of MCU components revealed topology-dependent interactions. We also determined whether MCUR1 and EMRE distribution at the subcellular level is exclusive for mitochondria. An intensity profile analysis of the BiFC signal revealed near-complete overlay of both BiFC and TMRM fluorescence, suggesting that most of the MCUR1 and EMRE complex formation occurs in the mitochondria (Figure 3C). Based on these findings, several issues must be addressed to determine whether and how the distribution of the heterooligomeric MCU complex is involved in opening MCU channels. First does MCUR1-EMRE accumulate in puncta enough to rapidly activate the MCU channel? To address this question, we visualized the BiFC signals at higher resolution to monitor MCU complex distribution in HeLa cells (Figure 3D). The MCUR1-EMRE BiFC distributed into puncta over TMRM, supporting the idea that MCUR1 is required for MCU complex. Having observed that MCUR1-EMRE forms a puncta, we tested whether the loss of MCUR1 impacts oligomeric MCU distribution. The formation of MCU puncta was markedly reduced in cells lacking MCUR1 (Figure 3E). Collectively, these results indicate that MCUR1 is necessary for MCU complex formation.

Loss of MCUR1 Disrupts MCU Complex Assembly

The observation that MCUR1 binds with MCU and EMRE led us to explore MCUR1-dependent MCU complex assembly by blue native (BN)-PAGE and FPLC (fast protein liquid chromatography) analysis. To examine the size of the MCU complex produced by the interaction of MCU and its regulators, total cell lysates were analyzed by size exclusion chromatography. We transfected HEK293T wild-type (WT) cells with MCU alone or in combinations of MCU with MCUR1. Fractions from a FLAG-tagged MCU-expressed sample revealed oligomers with apparent molecular mass between ~670 and 44 kDa (Figures 4A and 4B, top). However, V5-MCUR1 alone appeared as a low-order oligomeric complex (Figures 4A and 4B, top). Because MCU and MCUR1 interact, the coexpression may stabilize higher order oligomeric forms. When MCU was cotransfected with MCUR1, probing for both MCU and MCUR1 revealed a higher order oligomeric size, indicating that MCUR1 binds with MCU and that, likely, the binding is a determinant of MCU oligomerization (Figures 4A and 4B, middle). We also tested whether the loss of MICU1 affects MCU higher order oligomerization. The formation of higher order MCU oligomer is unaffected in MICU1 KD cells, suggesting the MICU1 role for Ca^{2+} sensing and dynamic nature of the MCU and MICU1 complex (Figure 4A, bottom). These results indicate that MCU and MCUR1 are part of the MCU complex. Having observed the stabilization of the higher order oligomeric MCU complex in the presence of MCUR1, we examined whether the loss of MCUR1 results in low-order molecular MCU complex. To further establish that MCUR1 facilitates higher order oligomeric MCU complex, FLAG-tagged adenoviral-MCU (Ad-MCU) was expressed in $MCUR1^{\Delta EC}$ endothelial cells (Figure 4C). BN-PAGE and FPLC MCU fractionation profile analysis showed that loss of MCUR1 resulted in a significant disruption of MCU heterooligomeric size (Figures 4D–4F). These results indicate that MCU and MCUR1 are binding partners in the stable assembly of the MCU complex.

To identify the regions of MCUR1 and MCU that are determinants of interaction, we generated a series of MCU truncations and examined their ability to interact with MCUR1 in mitochondria. The truncated MCU-GFP constructs were generated by 71, 30, 31, and 7 (Δ1, Δ2, Δ3, and Δ4) amino acid deletions of full-length MCU (Figure 5A). To identify the interaction between the MCU regions and MCUR1, we ectopically expressed these MCU-GFP mutants individually or in combination with MCUR1-FLAG plasmid in COS-7 cells (Figure 5B, top and bottom left). Immunoprecipitation of MCU with an antibody specific for GFP, followed by western blotting, revealed that the Δ1 and Δ4 region corresponding to the MCU N-terminal domain (NTD) and coiled-coil domain of MCU is a determinant of MCUR1 binding (Figure 5B, top right). Having observed the MCU-MCUR1 determinant site of MCU, we systematically generated truncations of MCUR1-FLAG (ΔN20, Δ1, Δ2, Δ3, Δ1,2, and Δ2,3)

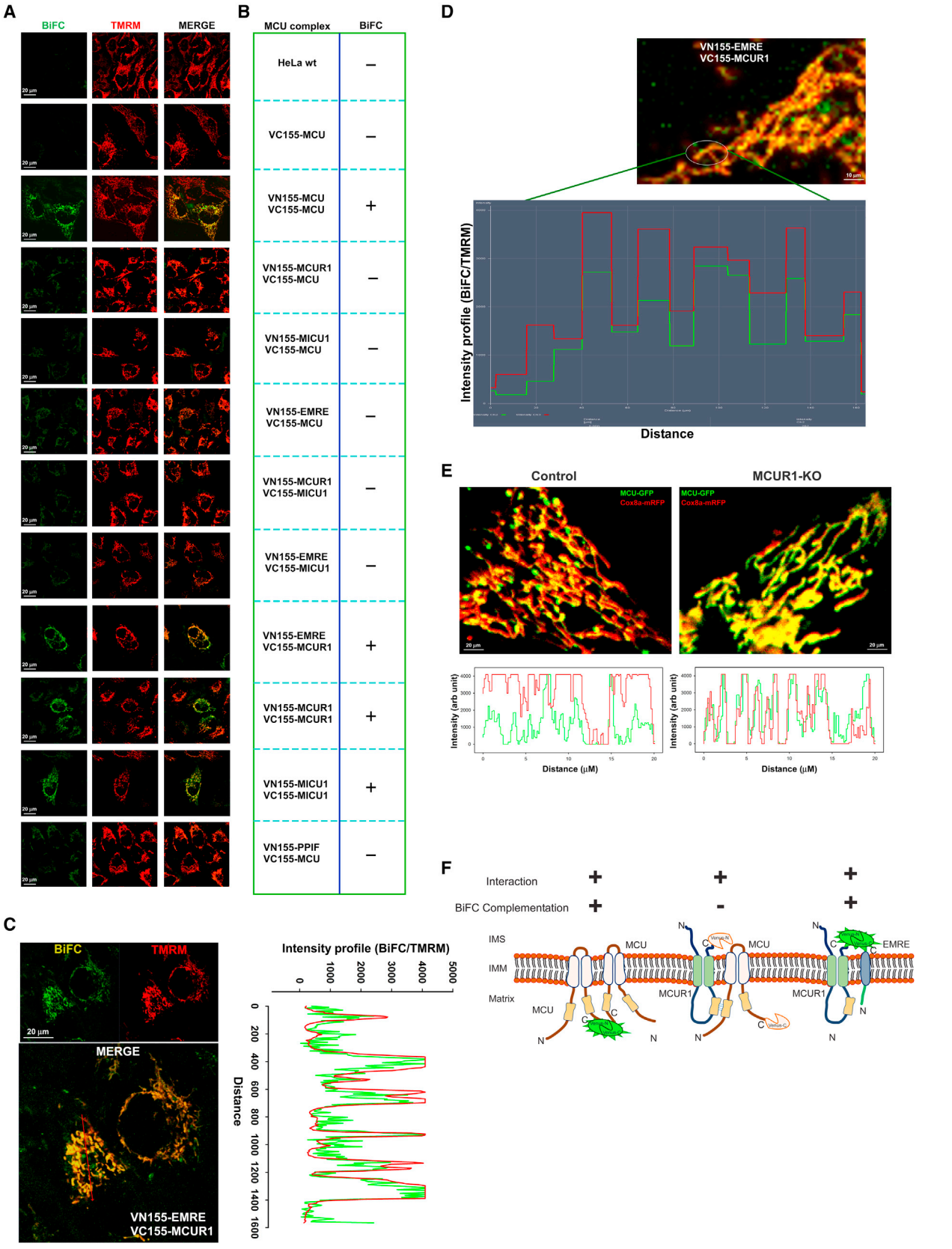

(legend on next page)

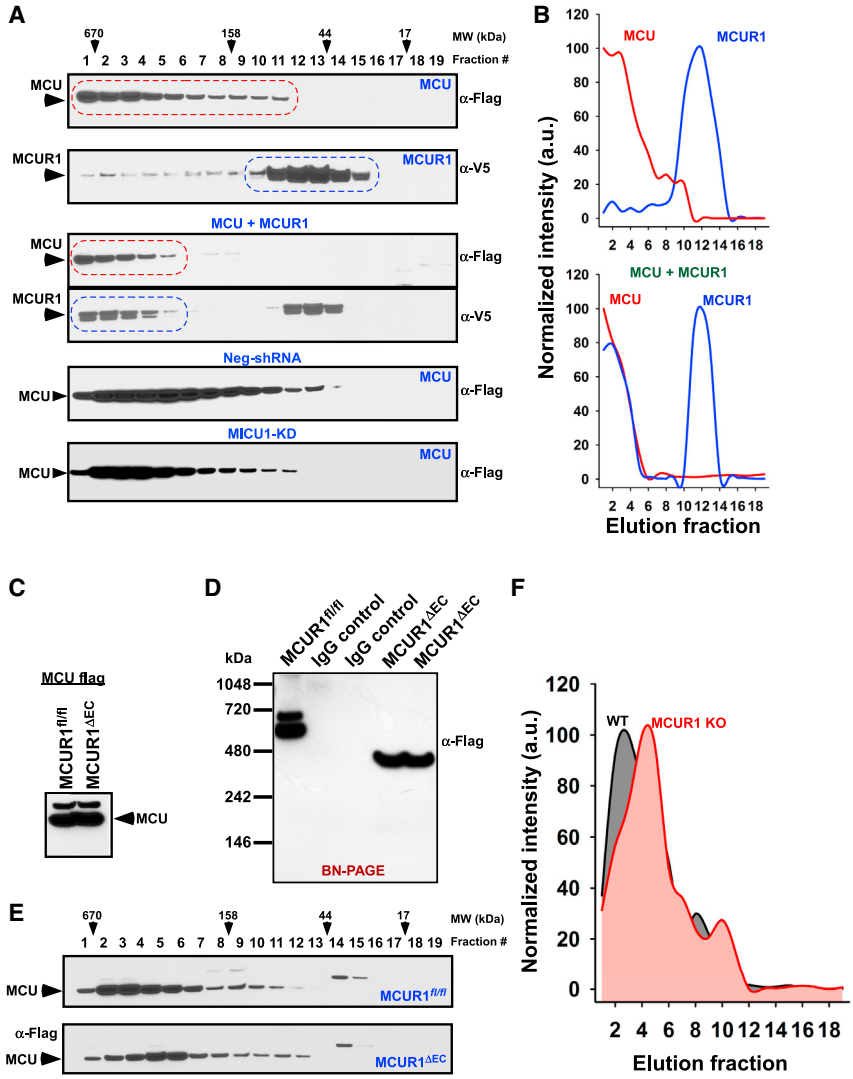

Figure 4. MCUR1 Is Required for MCU Complex Assembly

(A) HEK293T cells were transfected with MCU-FLAG or MCUR1-V5 alone and in combination, and cell lysates were subjected to FPLC analysis. FPLC fractions were probed with FLAG or V5 antibodies (top and middle). Neg-shRNA and MICU1 KD HEK293T cells were transfected with MCU-FLAG, and cell lysates were subjected to FPLC analysis. FPLC fractions were probed with FLAG antibody (bottom). (n = 3).

(B) MCU and MCUR1 protein elution profiles were quantified from (A) and expressed as normalized intensity.

(C)Western blot analysis of cell lysates from MCUR1$^{fl/fl}$ and MCUR1$^{\Delta EC}$ ECs transduced with Ad-MCU FLAG and probed with FLAG antibody.

(D) Ad-MCU-FLAG expressing MCUR1$^{fl/fl}$ and MCUR1$^{\Delta EC}$ EC lysates were immunopurified with FLAG antibody, and FLAG peptide (100 μg/ml; Sigma) was used to elute MCU-FLAG from affinity resins. The eluted immunoprecipitates were subjected to BN-PAGE and probed for FLAG antibody. IgG, immunoglobulin G.

(E) MCUR1$^{fl/fl}$ (top) and MCUR1$^{\Delta EC}$ (bottom) ECs expressing Ad-MCU-FLAG were lysed, cell lysates were separated on a Superdex 200 gel filtration column, and fractions were immunoblotted with FLAG antibody.

(F) The intensity profile of MCU protein band corresponding to the elution fraction number (n = 3).

(Figure 5C). Similarly, MCUR1 truncation mutants and full-length MCU-HA were co-expressed and subjected to immunoprecipitation using an antibody specific for HA (Figure 5D). Immunoprecipitation analysis indicated that MCUR1 Δ3, Δ1,2, and Δ2,3 failed to bind with MCU-HA, suggesting that the Δ3 region corresponding to the putative coiled-coil domain of MCUR1 is a binding determinant of MCU-MCUR1 (Figure 5D, top right). These results indicate that MCU and MCUR1 binding is determined through coiled-coil domain interactions.

Inhibition of MCU/MCUR1-Dependent $[Ca^{2+}]_m$ Uptake Perturbs Cellular Bioenergetics and Promotes Autophagy

Perturbation of $[Ca^{2+}]_m$ uptake may lead to cellular bioenergetic crisis (McCormack and Denton, 1990; Shanmughapriya et al., 2015b). To determine the effect of reduced $[Ca^{2+}]_m$ uptake, ATP levels in endothelial cells derived from MCUR1$^{\Delta EC}$ and MCU$^{\Delta EC}$ mice were examined. Consistent with reduced $[Ca^{2+}]_m$ uptake, basal ATP levels were significantly reduced in MCUR1$^{\Delta EC}$ and MCU$^{\Delta EC}$ endothelial cells (Figure 6A). Next, we examined whether agonist-induced $[Ca^{2+}]_m$ uptake affects ATP levels in endothelial cells derived from MCUR1$^{\Delta EC}$. Endothelial cells isolated from VE-Cre and MCUR1$^{\Delta EC}$ were stimulated with a GPCR agonist, thrombin, and ATP levels were measured. Upon stimulation, control cells

Figure 3. MCUR1 Binds MCU and EMRE to Form Complex Puncta in Mitochondria

(A and B) BiFC analysis to visualize MCU complex components on a single-cell basis. Representative confocal images of live HeLa cells transiently transfected with separated YFP fragments that were tagged at the C terminus of MCU complex components (Venus-N155 and Venus-C155) and stained with mitochondrial marker TMRM (n = 3–4).

(C) Spatial overlap and intensity profiles demonstrate mitochondrial co-localization of MCUR1 and EMRE (n = 3).

(D) Representative high-resolution confocal image depicts the MCUR1/EMRE complex puncta in mitochondria.

(E) Top: representative high-resolution confocal images of live mouse embryonic fibroblasts (MEFs) transiently cotransfected with MCU-GFP and Cox8a-mRFP in control and MCUR1 KO (n = 3). Bottom: spatial overlap and intensity profiles.

(F) Cartoon depicting the topology and interactions of MCU complex. IMS, inter-membrane space.

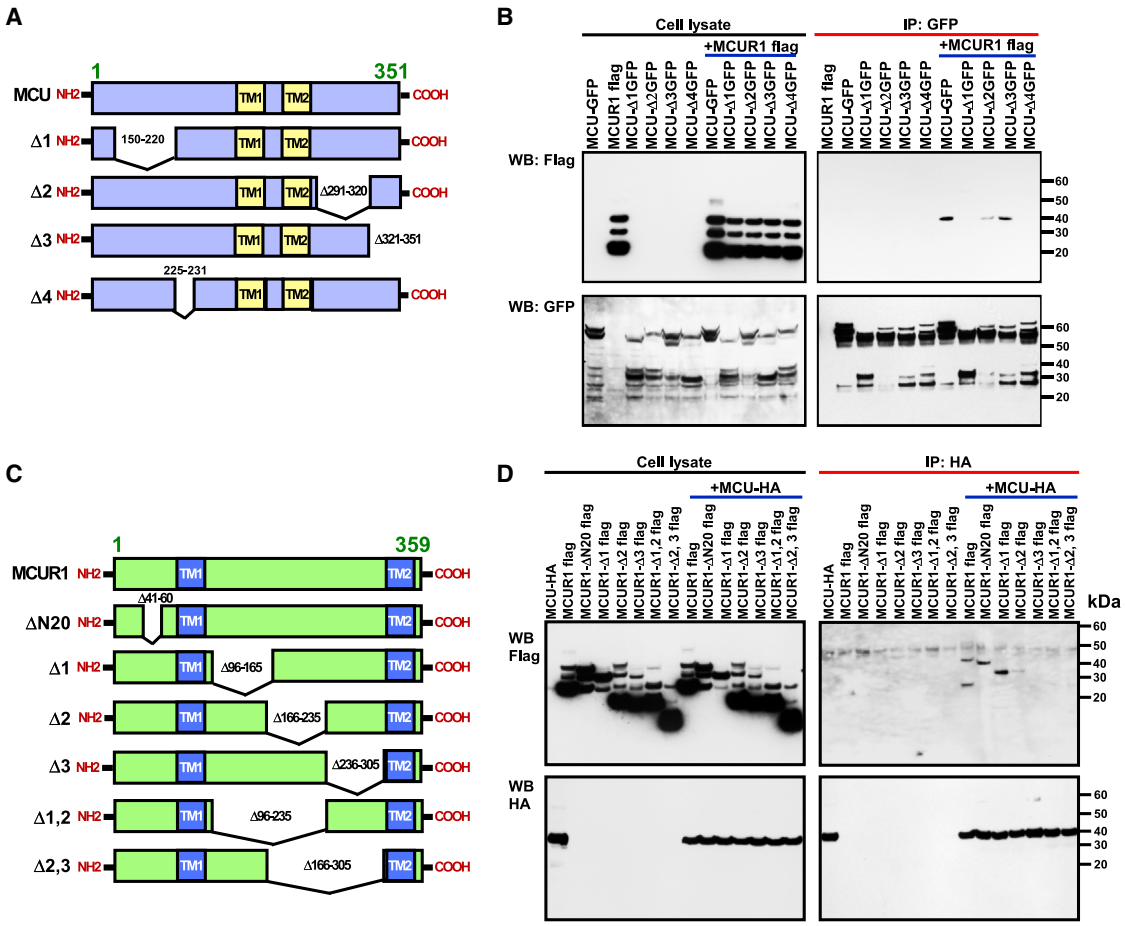

Figure 5. Coiled-Coil Domains of MCUR1 and MCU Are Determinants for MCU-MCUR1 Binding

(A) Schematic of full-length MCU with its functional domains and truncated versions of MCU (MCU Δ1–Δ4).

(B) Cell lysates (left) or immunoprecipitated material (IP; right) from COS-7 cells expressing MCU-GFP/MCUR1-FLAG or MCUR1-FLAG/MCU Δ1-Δ4-GFP either individually or in combination as indicated and immunoblotted for FLAG (top) and GFP (bottom) antibodies (n = 3). WB, western blot.

(C) Schematic of full-length MCUR1 with its functional domains and truncated versions of MCUR1 (ΔN20, MCUR1 Δ1–Δ3, MCUR1 Δ1,2, and MCUR1 Δ2,3).

(D) Cell lysates (left) or immunoprecipitated material (right) from COS-7 cells expressing MCU-HA/MCUR1-FLAG or MCU-HA/MCUR1-FLAG truncations either individually or in combination as indicated and immunoblotted for FLAG (top) and HA (bottom) antibodies (n = 3).

showed increased ATP levels when compared to MCUR1$^{\Delta EC}$ cells (Figure 6B). In contrast, mitochondrial-derived reactive oxygen species is considerably decreased, indicating that electron-transport complexes are intact (Figures 6C and 4D). Because $\Delta\Psi_m$ and oxygen consumption rate (OCR) are unaltered, we examined uncoupling protein (UCP)2 expression in MCUR1$^{\Delta EC}$ endothelial cells. UCP2 protein abundance was increased in MCUR1$^{\Delta EC}$ endothelial cells, suggesting that there is utilization of the H^+ gradient (Figure 6E). To further verify whether increased levels of UCP2 promotes mitochondrial proton leak, endothelial cells and cardiomyocytes from controls, MCUR1$^{\Delta EC}$, and cMCUR1 KO were subjected to proton leak measurement. Endothelial cells derived from MCUR1$^{\Delta EC}$ mice showed higher proton leak, indicating the possible utilization of proton gradient that prevents $\Delta\Psi_m$ hyperpolarization (Figures 6F and 6G). Given that UCP2 is widely distributed (Echtay et al., 2001), it is conceivable that the higher heat dissipation of MCUR1$^{\Delta EC}$ animals resulted from UCP2 upregulation. Next, we tested whether alteration of UCP2 levels affects the interaction between MCUR1 and MCU or EMRE. Scrambled and UCP2 siRNA (small interfering RNA)-treated HEK293T cells were single or cotransfected with MCUR1-V5 and MCU-FLAG or EMRE-FLAG plasmid constructs. The cell lysates were subjected to immunoprecipitation with antibody specific for V5 (Figure 6H). Immunoprecipitation analysis indicated that the interaction between MCUR1 and MCU or EMRE was unaffected, indicating that MCU complex assembly was independent of UCP2 abundance.

Having demonstrated that MCUR1 KO results in low cellular ATP, we postulated that alternative modes of cell survival may be upregulated. One such pathway that may be induced is autophagy (Cárdenas et al., 2010). To investigate whether autophagy is increased during mitochondrial MCU dysregulation, HeLa cells stably expressing Neg-shRNA (negative control short hairpin RNA) and MCUR1, LETM1, MCU, EMRE, and MICU1 shRNA were infected with Ad-LC3-GFP-RFP (red fluorescent protein). Loss of MCU complex components and LETM1 exhibited

elevated LC3 puncta and autophagy markers (Figures S3A–S3D). However, when cells were starved for 6 hr in Earle's balanced salt solution, the difference in the number of LC3 puncta between control and KD cells became less evident (Figures S3A–S3D). These KD results were further confirmed in MCUR1$^{\Delta EC}$ and MCU$^{\Delta EC}$ cells, where loss of MCUR1 and MCU resulted in an increased number of LC3 puncta and autophagy markers in endothelial cells (Figures 7A–7C). Ultrastructural analysis of cMCUR1 KO cardiomyocytes displayed a higher number of autophagosomes (Figure 7D, right). Loss of MCUR1 is associated with increased autophagy, resulting in fewer and elongated mitochondria within the sarcomere structure (Figures 7D and S4A). To determine whether the elevated autophagy was eliminated, we examined autophagy markers in MCUR1 or MCU KO endothelial cells after reconstitution of Ad-MCUR1 and Ad-MCU. As expected, reconstitution of MCUR1 and MCU in appropriate KO endothelial cells attenuated autophagy (Figures S4B–S4E). Together, these data establish that MCUR1 is required for MCU-dependent $[Ca^{2+}]_m$ uptake for normal cellular bioenergetics and cell function.

DISCUSSION

Several protein components have been identified as associating factors for MCU complex formation, and the majority are hydrophobic membrane proteins. Although their precise functions are still emerging, MICU1 is an EF-hand-containing mitochondrial protein that functions as a gatekeeper for MCU-mediated $[Ca^{2+}]_m$ uptake through its Ca^{2+} sensing function. The MICU1 paralogues MICU2 and MICU3 serve to play a reciprocal role in regulating MCU activity (Patron et al., 2014). EMRE is a single-pass transmembrane IMM protein that is necessary for MCU complex activity, but its precise role in MCU complex is unknown. MCUR1 was originally identified as a positive regulator of MCU complex through its interaction with core component MCU. Silencing of MCUR1 resulted in reduced MCU complex activity without affecting $\Delta\Psi_m$. Given that the establishment of the original biophysical characterization of MCU by using mitoplasts derived from cells (Kirichok et al., 2004), later work showed that purified recombinant MCU itself could reconstitute some single-channel-like properties but lacks typical single-channel behavior of the uniporter (De Stefani et al., 2011). Recent studies established that MCU regulatory components are necessary for the reconstitution of proper MCU activity (Chaudhuri et al., 2013; Csordás et al., 2013; Hoffman et al., 2013; Mallilankaraman et al., 2012a, 2012b; Raffaello et al., 2013; Sancak et al., 2013). To address this discrepancy, we generated the MCUR1 KO mice, and mitoplasts derived from cardiomyocytes clearly showed that the loss of MCUR1 significantly suppressed the I_{MCU}, indicating that MCUR1 is essential for proper MCU activity in situ.

Recently, the N-terminal domain of MCU was shown to be determinant of MCUR1 binding, but its regulatory role is unclear (Lee et al., 2015). Enigmatically, it has been postulated that MCUR1 participates as an assembly factor (Paupe et al., 2015). The BiFC and FPLC profile analysis of MCUR1, MCU, and EMRE led to MCUR1 characterization as an MCU complex scaffold factor. The precise mechanism by which MCUR1 functions as scaffold factor requires further research, but we show that MCUR1 stabilizes the subcomplexes, which may help to join them to other regulatory components such as EMRE in the full assembly of the mature complex. The role of MCUR1 as an MCU complex scaffold factor was supported by the FPLC and immune-affinity proteomic analyses. A number of features of MCUR1 suggest that it is involved in the assembly of the membrane components of the MCU complex. First, it contains two transmembrane and coiled-coil domains, which are necessary for protein-protein interaction. Second, the MCU complex fails to assemble fully in the absence of MCUR1. Additionally, loss of MCUR1 considerably reduced I_{MCU} current, suggesting that binding of MCUR1 with MCU is required for efficient MCU activity.

In the context of its functional role, lower ATP levels and autophagy progression in our MCUR1 KO models is possibly due to lack of MCU-dependent $[Ca^{2+}]_m$ uptake, which is required for the regulation of oxidative phosphorylation, F_1F_0-ATPase, and ANT (adenine nucleotide translocase) activities (Glancy and Balaban, 2012). Surprisingly, either KD or deletion of MCU or MCUR1 in multiple cell lines and animal models retained the normal $\Delta\Psi_m$, suggesting the utilization of proton gradient for other mechanisms. Our results indicate that loss of MCUR1 in endothelial cells resulted in UCP2 upregulation and higher heat generation. Given that ATP synthase activity is also modulated by Ca^{2+}, it is conceivable that UCP2 fluxes protons to prevent $\Delta\Psi_m$ hyperpolarization. Having observed the ATP decline followed by AMPK activation in MCU or MCUR1 KO ECs, it is tempting to speculate that the loss of MCU-dependent Ca^{2+} uptake may drive the metabolic switch of these cells. Although Ca^{2+}-dependent AMPK activation is known to promote autophagy, it has been proposed that ROS also promotes autophagy and apoptosis (Kaminskyy and Zhivotovsky, 2014). Our previous study revealed that loss of MICU1 promotes basal mitochondrial Ca^{2+} accumulation and mROS overproduction. The ROS elevation promotes sensitization of cells to injury (Mallilankaraman et al., 2012b). It is plausible that loss of MICU1 may promote ROS-dependent autophagy. We conclude, based on our in vivo and in vitro data, that MCUR1 assembles the MCU complex and regulates its function during cytosolic Ca^{2+} dynamics.

EXPERIMENTAL PROCEDURES

Additional information regarding animals; isolation of primary MPMVECs and MLF, HEK293T, HeLa, COS-7 cultures and generation of MCU complex stable KD cell lines; plasmids; buffers; antibodies; sample preparation; and cell permeabilization and detailed procedures are provided in the Supplemental Experimental Procedures.

Animals

Cardiac-specific *Mcur1* KOs were generated by crossing *Mcur1*$^{fl/fl}$ mice with αMHC-Cre. Similarly, endothelial-specific *Mcur1* and *MCU* KOs were generated by crossing of VE-Cre mice with *Mcur1*$^{fl/fl}$ and *Mcu*$^{fl/fl}$ mice, respectively. All animal experiments were approved by Temple University's Institutional Animal Care and Use Committee (IACUC) and followed AAALAC (Association for Assessment and Accreditation of Laboratory Animal Care International) guidelines. The detailed method for generating *Mcur1*$^{fl/fl}$ mice can be found in the Supplemental Experimental Procedures.

Metabolic Assessment of Mice

The metabolic status of MCUR1$^{fl/fl}$, MCUR1$^{\Delta EC}$, and cMCUR1-KO mice was assessed using a Comprehensive Laboratory Animal Monitoring System

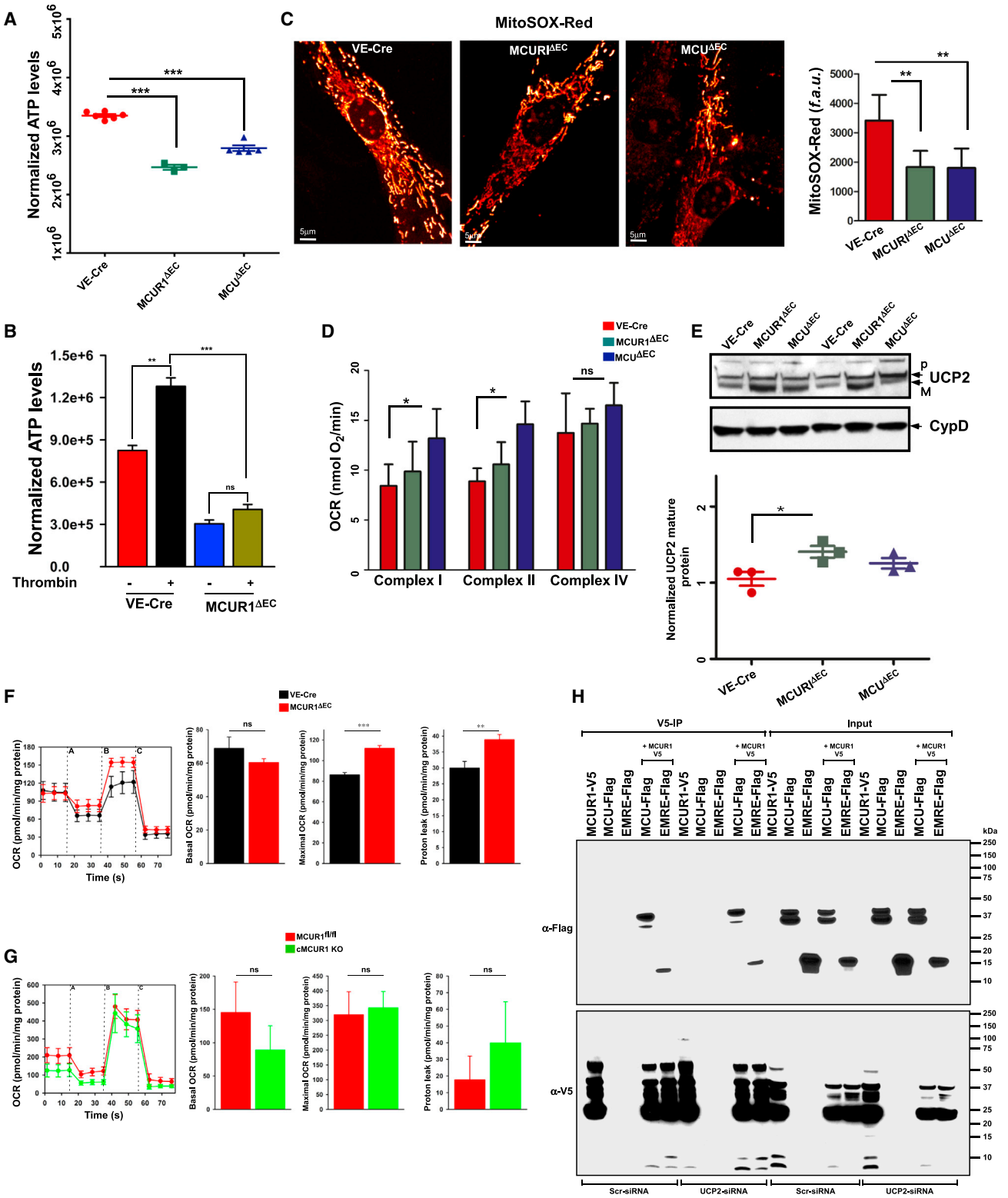

Figure 6. Disruption of MCU-Dependent $[Ca^{2+}]_m$ Uptake Perturbs Endothelial Cellular Bioenergetics

(A) Scatterplot of cellular ATP levels in VE-Cre, MCUR1$^{\Delta EC}$, and MCU$^{\Delta EC}$ ECs. Data indicate mean ± SEM. ***p < 0.001; n = 3–6.

(B) Bar graph represents cellular ATP levels in VE-Cre and MCUR1$^{\Delta EC}$ ECs after stimulation with thrombin (500 mU/ml). Data indicate mean ± SEM. **p < 0.01; ***p < 0.001; ns, not significant; n = 4.

(legend continued on next page)

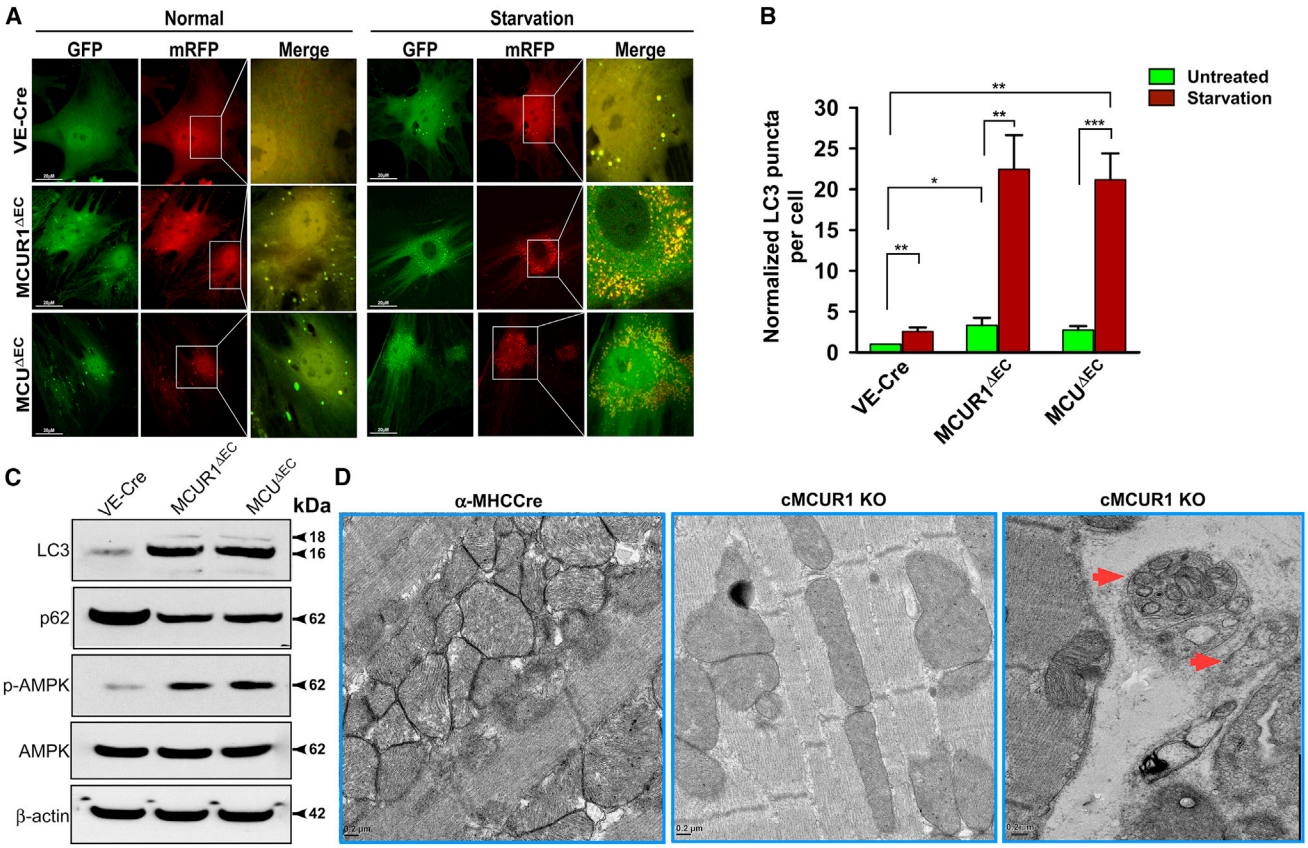

Figure 7. Dysregulation of MCU-Dependent $[Ca^{2+}]_m$ Uptake Triggers Autophagy

(A) Representative confocal images of mRFP-GFP tandem fluorescent-tagged LC3 (tfLC3) in VE-Cre, MCUR1$^{\Delta EC}$, and MCU$^{\Delta EC}$ ECs with and without starvation (n = 4).

(B) Quantification of normalized LC3 puncta in VE-Cre, MCUR1$^{\Delta EC}$, and MCU$^{\Delta EC}$ ECs. Data indicate mean ± SEM. *p < 0.05; **p < 0.01; ***p < 0.001; n = 4.

(C) Western blot analysis of cell lysates from VE-Cre, MCUR1$^{\Delta EC}$, and MCU$^{\Delta EC}$ ECs and cell lysates probed for LC3, p62, pAMPK, and AMPK antibodies. β-actin served as loading control (n = 3).

(D) Electron micrograph of heart sections of αMHCCre (left) and cMCUR1 KO (middle). The cMCUR1 KO image depicts the accumulation of autophagosomes (red arrows, right) (two mice per group).

(CLAMS; Columbus Instruments). Details can be found in the Supplemental Experimental Procedures.

Mitoplast Patch-Clamp Recording

Mitoplast patch-clamp recordings were performed at 30°C, as detailed previously (Chaudhuri et al., 2013; Hoffman et al., 2013; Joiner et al., 2012; Kirichok et al., 2004), with the following modifications. Freshly prepared mitoplasts were placed on Cell-Tak-coated coverslips and mounted on the microscope. Mitoplasts isolated from cardiomyocytes of WT, αMHCCre, and cMCUR1 KO mice were bathed in a solution containing sodium gluconate (150 mM), KCl (5.4 mM), $CaCl_2$ (5 mM), and HEPES (10 mM) (pH 7.2). The pipette solution contained sodium gluconate (150 mM), NaCl (5 mM), sucrose (135 mM), HEPES (10 mM), and EGTA (1.5 mM) (pH 7.2). After formation of GΩ seals (20 to 35 MΩ), the mitoplasts were ruptured with a 200- to 400-mV pulse for 2 to 6 ms. Mitoplast capacitance was measured (2.5 to 3.0 pF). After capacitance compensation, mitoplasts were held at 0 mV, and I_{MCU} was elicited with a

(C) Representative confocal images showing MitoSOX Red fluorescence in VE-Cre, MCUR1$^{\Delta EC}$, and MCU$^{\Delta EC}$ ECs. Quantification of MitoSOX Red fluorescence in VE-Cre, MCUR1$^{\Delta EC}$, and MCU$^{\Delta EC}$ ECs. Data indicate mean ± SEM. **p < 0.01; n = 3; f.a.u., fluorescence a.u.

(D) Bar graph represents complex-I-, II-, and IV-mediated oxygen consumption rate (OCR) in VE-Cre, MCUR1$^{\Delta EC}$, and MCU$^{\Delta EC}$ ECs. Data indicate mean ± SEM. *p < 0.05; ns, not significant; n = 3–4.

(E) Western blot analysis of cell lysates from VE-Cre, MCUR1$^{\Delta EC}$, and MCU$^{\Delta EC}$ ECs and probed for UCP2 antibody. Cyclophilin D (CypD) served as the loading control. Quantification of normalized UCP2 protein abundance in VE-Cre, MCUR1$^{\Delta EC}$ and MCU$^{\Delta EC}$ ECs. Data indicate mean ± SEM. *p < 0.05; n = 3. p, processed; M, matured.

(F and G) Oxygen consumption rate (OCR) was measured in VE-Cre, MCUR1$^{\Delta EC}$, MCUR1$^{fl/fl}$, and cMCUR1 KO cells. After basal OCR was measured, oligomycin, FCCP, and rotenone + antimycin A were added as indicated. Bars represent mean basal OCR, maximal OCR, and proton leak. Data indicate mean ± SEM. **p < 0.01; ***p < 0.001; ns, not significant; n = 8.

(H) Forty-eight hours post-transfection with siRNA as indicated, HEK293T cells were cotransfected with MCUR1-V5 and MCU-FLAG or EMRE-FLAG plasmids. Cell lysates (right) or immunoprecipitated material (IP; left) from 293T cells expressing MCUR1-V5/MCU-FLAG or MCUR1-V5/EMRE-FLAG either individually or in combination as indicated and immunoblotted for FLAG (top) and V5 (bottom) antibodies (n = 3). Scr, scrambled.

voltage ramp (from −160 to 80 mV, 120 mV/s). Samples were discarded if the break-in took longer than 5 s after the addition of 5 mM Ca^{2+}. Currents were recorded using an Axon200B patch-clamp amplifier with a Digidata 1320A acquisition board (pCLAMP 10.0 software; Axon Instruments). The external/bath solution (5 mM Ca^{2+}) was chosen on the basis of previous measurements (Hoffman et al., 2013).

Ca^{2+} Uptake and $\Delta\Psi_m$ Measurement in Permeabilized Cells

The simultaneous measurement of $\Delta\Psi_m$ and extramitochondrial Ca^{2+} ($[Ca^{2+}]_{out}$) clearance was achieved by loading the permeabilized cells with JC-1 (800 nM) and Fura-2FF (0.5 μM), respectively, as described earlier (Mallilankaraman et al., 2012a; Shanmughapriya et al., 2015a). Details can be found in the Supplemental Experimental Procedures.

BiFC Assay

To visualize protein binding, plasmids were created for BiFC of Venus using N-terminal (VN) and C-terminal (VC) reporter fragments, as previously described (Kodama and Hu, 2010). In brief, the coding region of each cDNA (MCUR1, MCU, MICU1, EMRE, and PPIF) was amplified by PCR and cloned into pBiFC-VC155 (Addgene plasmid 22011) to generate the corresponding cDNA-VC protein expressed in frame. Similarly, all the cDNAs were also cloned into pBiFC-VN155 (Addgene plasmid 27097) to generate the corresponding cDNA-VN protein expressed in frame. HeLa cells were plated in six-well plates containing 0.2% gelatin-coated glass coverslips and transfected with corresponding plasmid encoding for MCU complex component proteins fused with VN and VC reporter fragments. After 36 hr, cells were loaded with tetramethylrhodamine, methyl ester (TMRM; 100 nM) for 30 min at 37°C for mitochondrial staining. Note: Basal autofluorescence was observed in non-expressing cells that was considered negative. Image acquisition was performed using a Carl Zeiss 510 confocal microscope using a 63× oil objective with excitation at 514 and 561 nm. Intensity profiles were created using line scans for relative fluorescence of BiFC/TMRE using Carl Zeiss ZEN 2010 imaging software.

Size Exclusion Chromatographic Analysis of MCU Complex

The single or co-transfected HEK293T cleared cell lysates were directly loaded onto a Superdex 200 FPLC column (ÄKTA Pure FPLC; GE Healthcare) at a flow rate of 0.5 ml/min (Park et al., 2009; Shanmughapriya et al., 2015a). Fractions were collected and analyzed for MCU complex. Details can be found in the Supplemental Experimental Procedures.

Proteomic Analysis of MCUR1 Interacting Proteins

The MCUR1-FLAG immunoprecipitated products were identified by label-free proteomics (PAGE followed by liquid chromatography-tandem mass spectrometry; GeLC-MS/MS), as previously described (Boden et al., 2015). Details can be found in the Supplemental Experimental Procedures.

Autophagy

Autophagy was monitored using monomeric RFP (mRFP)-GFP-LC3 confocal microscopy and p62 and LC3 immunoblotting. Details can be found in the Supplemental Experimental Procedures.

Statistical Analysis

Data were expressed as mean ± SE. Statistical significance was evaluated via Student's unpaired t test and one-way and two-way ANOVAs. $p < 0.05$ was considered statistically significant. All experiments were conducted at least three times, unless specified. Data were plotted either with Sigma Plot 11.0 software or GraphPad Prism version 6 software.

SUPPLEMENTAL INFORMATION

Supplemental Information includes Supplemental Experimental Procedures, four figures, and one table and can be found with this article online at http://dx.doi.org/10.1016/j.celrep.2016.04.050.

AUTHOR CONTRIBUTIONS

D.T., Z.D., S.S., D.A.K., N.E.H., N.N., J.P.F., A.R.C., M.E.R., S.R., and M.M. performed and analyzed experiments involving biochemical, molecular, and cellular experiments. T.T., S.J.G., S.L.B., D.P.C., P.S., and S.R. performed molecular cloning and BiFC experiments. D.T., C.B., and S.M. performed proteomic experiments. X.Z., J.S., and J.Y.C. performed cardiomyocyte isolation and electrophysiology experiments. D.A.K. and A.D. performed isolation of primary endothelial cells, proliferation, and migration analysis. S.A.T., F.J., and V.M.G. performed OXPHOS complex analysis. J.C., J.H., and V.P. performed histology and electron microscopy analysis. J.E.R. generated adenoviral constructs. T.S.L. and J.W.E. generated $MCU^{fl/fl}$ mice. D.T., S.R., and R.S.A. performed mouse metabolic profile experiments and analysis. S.R., S.R.H., S.M.S., and W.J.K. generated cardiac-specific MCUR1 KO mice and interpreted experiments and data. D.T., Z.D., S.S., S.R., D.A.K., and M.M. conceived, designed, analyzed, and interpreted experiments and data. D.T., S.S., S.R., D.A.K., and M.M. wrote the manuscript, with contributions from all authors.

ACKNOWLEDGMENTS

We thank Chang-Deng Hu for sharing BiFC plasmid constructs. We also thank Jean L. Ross and Shannon Modla for electron microscopy sample preparation and image acquisition. This research was funded by grants from the NIH (R01GM109882, R01HL086699, R01HL119306, and 1S10RR027327 to M.M.; R01GM111672 to V.M.G.; and P01 DA037830, principal investigator, K. Khalili). Z.D. is supported by the China Scholarship Council (no. 201403170252). V.M.G. is supported by a grant (A-1810) from The Welch Foundation. F.J. is supported by FONDECYT postdoctoral fellowship # 3140458. Metabolic profiling was performed by the University of Pennsylvania Diabetes Research Center, Mouse Phenotyping, Physiology and Metabolism Core (NIH grant P30-DK19525). Access to electron microscopy was supported by NIH-NIGMS (P20 GM103446) and the NSF (IIA-1301765).

Received: January 26, 2016
Revised: March 5, 2016
Accepted: April 12, 2016
Published: May 12, 2016

REFERENCES

Babcock, D.F., Herrington, J., Goodwin, P.C., Park, Y.B., and Hille, B. (1997). Mitochondrial participation in the intracellular Ca2+ network. J. Cell Biol. *136*, 833–844.

Baughman, J.M., Perocchi, F., Girgis, H.S., Plovanich, M., Belcher-Timme, C.A., Sancak, Y., Bao, X.R., Strittmatter, L., Goldberger, O., Bogorad, R.L., et al. (2011). Integrative genomics identifies MCU as an essential component of the mitochondrial calcium uniporter. Nature *476*, 341–345.

Boden, G., Homko, C., Barrero, C.A., Stein, T.P., Chen, X., Cheung, P., Fecchio, C., Koller, S., and Merali, S. (2015). Excessive caloric intake acutely causes oxidative stress, GLUT4 carbonylation, and insulin resistance in healthy men. Sci. Transl. Med. *7*, 304re7.

Carafoli, E., and Lehninger, A.L. (1971). A survey of the interaction of calcium ions with mitochondria from different tissues and species. Biochem. J. *122*, 681–690.

Cárdenas, C., Miller, R.A., Smith, I., Bui, T., Molgó, J., Müller, M., Vais, H., Cheung, K.H., Yang, J., Parker, I., et al. (2010). Essential regulation of cell bioenergetics by constitutive InsP3 receptor Ca2+ transfer to mitochondria. Cell *142*, 270–283.

Chaudhuri, D., Sancak, Y., Mootha, V.K., and Clapham, D.E. (2013). MCU encodes the pore conducting mitochondrial calcium currents. eLife *2*, e00704.

Csordás, G., Golenár, T., Seifert, E.L., Kamer, K.J., Sancak, Y., Perocchi, F., Moffat, C., Weaver, D., de la Fuente Perez, S., Bogorad, R., et al. (2013). MICU1 controls both the threshold and cooperative activation of the mitochondrial Ca^{2+} uniporter. Cell Metab. *17*, 976–987.

Davidson, S.M., and Duchen, M.R. (2007). Endothelial mitochondria: contributing to vascular function and disease. Circ. Res. *100*, 1128–1141.

De Stefani, D., Raffaello, A., Teardo, E., Szabò, I., and Rizzuto, R. (2011). A forty-kilodalton protein of the inner membrane is the mitochondrial calcium uniporter. Nature *476*, 336–340.

Drago, I., Pizzo, P., and Pozzan, T. (2011). After half a century mitochondrial calcium in- and efflux machineries reveal themselves. EMBO J. *30*, 4119–4125.

Duchen, M.R. (2000). Mitochondria and calcium: from cell signalling to cell death. J. Physiol. *529*, 57–68.

Echtay, K.S., Winkler, E., Frischmuth, K., and Klingenberg, M. (2001). Uncoupling proteins 2 and 3 are highly active H(+) transporters and highly nucleotide sensitive when activated by coenzyme Q (ubiquinone). Proc. Natl. Acad. Sci. USA *98*, 1416–1421.

Fieni, F., Lee, S.B., Jan, Y.N., and Kirichok, Y. (2012). Activity of the mitochondrial calcium uniporter varies greatly between tissues. Nat. Commun. *3*, 1317.

Glancy, B., and Balaban, R.S. (2012). Role of mitochondrial Ca2+ in the regulation of cellular energetics. Biochemistry *51*, 2959–2973.

Gunter, T.E., and Pfeiffer, D.R. (1990). Mechanisms by which mitochondria transport calcium. Am. J. Physiol. *258*, C755–C786.

Hajnóczky, G., Robb-Gaspers, L.D., Seitz, M.B., and Thomas, A.P. (1995). Decoding of cytosolic calcium oscillations in the mitochondria. Cell *82*, 415–424.

Hoffman, N.E., Chandramoorthy, H.C., Shamugapriya, S., Zhang, X., Rajan, S., Mallilankaraman, K., Gandhirajan, R.K., Vagnozzi, R.J., Ferrer, L.M., Sreekrishnanilayam, K., et al. (2013). MICU1 motifs define mitochondrial calcium uniporter binding and activity. Cell Rep. *5*, 1576–1588.

Joiner, M.L., Koval, O.M., Li, J., He, B.J., Allamargot, C., Gao, Z., Luczak, E.D., Hall, D.D., Fink, B.D., Chen, B., et al. (2012). CaMKII determines mitochondrial stress responses in heart. Nature *491*, 269–273.

Kamer, K.J., and Mootha, V.K. (2014). MICU1 and MICU2 play nonredundant roles in the regulation of the mitochondrial calcium uniporter. EMBO Rep. *15*, 299–307.

Kamer, K.J., and Mootha, V.K. (2015). The molecular era of the mitochondrial calcium uniporter. Nat. Rev. Mol. Cell Biol. *16*, 545–553.

Kaminskyy, V.O., and Zhivotovsky, B. (2014). Free radicals in cross talk between autophagy and apoptosis. Antioxid. Redox Signal. *21*, 86–102.

Kirichok, Y., Krapivinsky, G., and Clapham, D.E. (2004). The mitochondrial calcium uniporter is a highly selective ion channel. Nature *427*, 360–364.

Kodama, Y., and Hu, C.D. (2010). An improved bimolecular fluorescence complementation assay with a high signal-to-noise ratio. Biotechniques *49*, 793–805.

Kwong, J.Q., Lu, X., Correll, R.N., Schwanekamp, J.A., Vagnozzi, R.J., Sargent, M.A., York, A.J., Zhang, J., Bers, D.M., and Molkentin, J.D. (2015). The mitochondrial calcium uniporter selectively matches metabolic output to acute contractile stress in the heart. Cell Rep. *12*, 15–22.

Lee, Y., Min, C.K., Kim, T.G., Song, H.K., Lim, Y., Kim, D., Shin, K., Kang, M., Kang, J.Y., Youn, H.S., et al. (2015). Structure and function of the N-terminal domain of the human mitochondrial calcium uniporter. EMBO Rep. *16*, 1318–1333.

Luongo, T.S., Lambert, J.P., Yuan, A., Zhang, X., Gross, P., Song, J., Shanmughapriya, S., Gao, E., Jain, M., Houser, S.R., et al. (2015). The mitochondrial calcium uniporter matches energetic supply with cardiac workload during stress and modulates permeability transition. Cell Rep. *12*, 23–34.

Mallilankaraman, K., Cárdenas, C., Doonan, P.J., Chandramoorthy, H.C., Irrinki, K.M., Golenár, T., Csordás, G., Madireddi, P., Yang, J., Müller, M., et al. (2012a). MCUR1 is an essential component of mitochondrial Ca2+ uptake that regulates cellular metabolism. Nat. Cell Biol. *14*, 1336–1343.

Mallilankaraman, K., Doonan, P., Cárdenas, C., Chandramoorthy, H.C., Müller, M., Miller, R., Hoffman, N.E., Gandhirajan, R.K., Molgó, J., Birnbaum, M.J., et al. (2012b). MICU1 is an essential gatekeeper for MCU-mediated mitochondrial Ca(2+) uptake that regulates cell survival. Cell *151*, 630–644.

McCormack, J.G., and Denton, R.M. (1990). Intracellular calcium ions and intramitochondrial Ca2+ in the regulation of energy metabolism in mammalian tissues. Proc. Nutr. Soc. *49*, 57–75.

Nicholls, D.G. (2005). Mitochondria and calcium signaling. Cell Calcium *38*, 311–317.

O'Rourke, B. (2007). Mitochondrial ion channels. Annu. Rev. Physiol. *69*, 19–49.

Pan, X., Liu, J., Nguyen, T., Liu, C., Sun, J., Teng, Y., Fergusson, M.M., Rovira, I.I., Allen, M., Springer, D.A., et al. (2013). The physiological role of mitochondrial calcium revealed by mice lacking the mitochondrial calcium uniporter. Nat. Cell Biol. *15*, 1464–1472.

Park, C.Y., Hoover, P.J., Mullins, F.M., Bachhawat, P., Covington, E.D., Raunser, S., Walz, T., Garcia, K.C., Dolmetsch, R.E., and Lewis, R.S. (2009). STIM1 clusters and activates CRAC channels via direct binding of a cytosolic domain to Orai1. Cell *136*, 876–890.

Patron, M., Checchetto, V., Raffaello, A., Teardo, E., Vecellio Reane, D., Mantoan, M., Granatiero, V., Szabò, I., De Stefani, D., and Rizzuto, R. (2014). MICU1 and MICU2 finely tune the mitochondrial Ca2+ uniporter by exerting opposite effects on MCU activity. Mol. Cell *53*, 726–737.

Paupe, V., Prudent, J., Dassa, E.P., Rendon, O.Z., and Shoubridge, E.A. (2015). CCDC90A (MCUR1) is a cytochrome c oxidase assembly factor and not a regulator of the mitochondrial calcium uniporter. Cell Metab. *21*, 109–116.

Perocchi, F., Gohil, V.M., Girgis, H.S., Bao, X.R., McCombs, J.E., Palmer, A.E., and Mootha, V.K. (2010). MICU1 encodes a mitochondrial EF hand protein required for Ca(2+) uptake. Nature *467*, 291–296.

Petrungaro, C., Zimmermann, K.M., Küttner, V., Fischer, M., Dengjel, J., Bogeski, I., and Riemer, J. (2015). The Ca(2+)-dependent release of the Mia40-induced MICU1-MICU2 dimer from MCU regulates mitochondrial Ca(2+) uptake. Cell Metab. *22*, 721–733.

Plovanich, M., Bogorad, R.L., Sancak, Y., Kamer, K.J., Strittmatter, L., Li, A.A., Girgis, H.S., Kuchimanchi, S., De Groot, J., Speciner, L., et al. (2013). MICU2, a paralog of MICU1, resides within the mitochondrial uniporter complex to regulate calcium handling. PLoS ONE *8*, e55785.

Raffaello, A., De Stefani, D., Sabbadin, D., Teardo, E., Merli, G., Picard, A., Checchetto, V., Moro, S., Szabò, I., and Rizzuto, R. (2013). The mitochondrial calcium uniporter is a multimer that can include a dominant-negative pore-forming subunit. EMBO J. *32*, 2362–2376.

Rasmussen, T.P., Wu, Y., Joiner, M.L., Koval, O.M., Wilson, N.R., Luczak, E.D., Wang, Q., Chen, B., Gao, Z., Zhu, Z., et al. (2015). Inhibition of MCU forces extramitochondrial adaptations governing physiological and pathological stress responses in heart. Proc. Natl. Acad. Sci. USA *112*, 9129–9134.

Rizzuto, R., De Stefani, D., Raffaello, A., and Mammucari, C. (2012). Mitochondria as sensors and regulators of calcium signalling. Nat. Rev. Mol. Cell Biol. *13*, 566–578.

Sancak, Y., Markhard, A.L., Kitami, T., Kovács-Bogdán, E., Kamer, K.J., Udeshi, N.D., Carr, S.A., Chaudhuri, D., Clapham, D.E., Li, A.A., et al. (2013). EMRE is an essential component of the mitochondrial calcium uniporter complex. Science *342*, 1379–1382.

Santo-Domingo, J., and Demaurex, N. (2012). Perspectives on: SGP symposium on mitochondrial physiology and medicine: the renaissance of mitochondrial pH. J. Gen. Physiol. *139*, 415–423.

Shanmughapriya, S., Rajan, S., Hoffman, N.E., Higgins, A.M., Tomar, D., Nemani, N., Hines, K.J., Smith, D.J., Eguchi, A., Vallem, S., et al. (2015a). SPG7 is an essential and conserved component of the mitochondrial permeability transition pore. Mol. Cell *60*, 47–62.

Shanmughapriya, S., Rajan, S., Hoffman, N.E., Zhang, X., Guo, S., Kolesar, J.E., Hines, K.J., Ragheb, J., Jog, N.R., Caricchio, R., et al. (2015b). Ca2+ signals regulate mitochondrial metabolism by stimulating CREB-mediated expression of the mitochondrial Ca2+ uniporter gene MCU. Sci. Signal. *8*, ra23.

Vais, H., Tanis, J.E., Müller, M., Payne, R., Mallilankaraman, K., and Foskett, J.K. (2015). MCUR1, CCDC90A, is a regulator of the mitochondrial calcium uniporter. Cell Metab. *22*, 533–535.

Williams, G.S., Boyman, L., Chikando, A.C., Khairallah, R.J., and Lederer, W.J. (2013). Mitochondrial calcium uptake. Proc. Natl. Acad. Sci. USA *110*, 10479–10486.